

# On-chip acidification rate measurements from single cardiac cells confined in sub-nanoliter volumes

Igor A. Ges · Igor A. Dzhura · Franz J. Baudenbacher

Published online: 24 January 2008  
© Springer Science + Business Media, LLC 2007

**Abstract** The metabolic activity of cells can be monitored by measuring the pH in the extracellular environment. Microfabrication and microfluidic technologies allow the sensor size and the extracellular volumes to be comparable to single cells. A glass substrate with thin film pH sensitive IrO<sub>x</sub> electrodes was sealed to a replica-molded polydimethylsiloxane (PDMS) microfluidic network with integrated valves. The device, termed NanoPhysiometer, allows the trapping of single cardiac myocytes and the measurement of the pH in a detection volume of 0.36 nL. For wild-type (WT) single cardiac myocytes an acidification rate of 6.45±0.38 mpH/min was measured in comparison to 19.5±0.38 mpH/min for very long chain Acyl-CoA dehydrogenase (VLCAD) deficient mice in 0.8 mM of Ca<sup>2+</sup>. VLCAD deficiency is a fatty acid oxidation disease leading to cardiomyopathy and arrhythmias. The acidification rate increased to 11.96±1.33 mpH/min for WT and to 32.0±4.64 mpH/min for VLCAD <sup>-/-</sup> in 1.8 mM of Ca<sup>2+</sup>. The NanoPhysiometer concept can be extended to study ischemia/reperfusion injury or disorders of other biological systems to identify strategies for treatment and possible pharmacological targets.

**Keywords** Microfluidic device · pH sensor · Iridium oxide films · Cardiac myocyte cells · Single cell manipulation · VLCAD · NanoPhysiometer

## 1 Introduction

Cell physiology is governed by adenosine triphosphate (ATP) consumption, which is tightly coupled to the metabolic activity of cells. The metabolic activity of cells can be monitored by measuring the acidification rate in the extracellular environment; therefore, changes in the biological function and the response to ligand binding to surface receptors, and the impact of chemicals and drugs on cell physiology can be studied by measuring the decrease in pH that occurs as acidic metabolites build up in the extracellular space (Lorenzelli et al., 2003; Parak et al., 2000; Thedinga et al., 2007).

A commercially available instrument, the Cytosensor Microphysiometer (Molecular Devices, Inc.), is used to measure extracellular pH on (typically) 10<sup>5</sup> cells in μl culture volumes using a Light Addressable Potentiometric Sensor to determine acidification rates in order to assess the metabolic activity of cells during pharma- or toxicological studies (Eklund et al., 2003; Hafner, 2000; Owicki et al., 1994).

To record metabolic changes of a small number or single cells it is necessary to scale down the cell culture volume and the sensor size and provide fluidic access to the cell culture volume for perfusion and toxin delivery (Shim et al., 2003). Recently, microfabrication and microfluidic technologies have been utilized to develop lab-on-a-chip devices for cell analysis in which the extracellular volume and the sensor size is smaller than or comparable to the cell size approaching *in vivo* conditions (Cheng et al., 2006; Ganitkevich et al., 2006b). Furthermore, single cell analysis in small volumes provides the opportunity for more detailed information on cells that are difficult to culture or are rare, and a more sensitive analysis with a higher temporal resolution than measurements on populations of cells. Single

I. A. Ges · I. A. Dzhura · F. J. Baudenbacher (✉)  
Department of Biomedical Engineering, Vanderbilt University,  
Nashville, TN, USA  
e-mail: f.baudenbacher@vanderbilt.edu

cell studies in oil-sealed restricted volumes on amperometric sensors have shown the release of lactate or purine from single cardiac myocytes (Bratten et al., 1998; Cai et al., 2002); however, this approach does not allow small extracellular volumes, the chemical control, and the perfusion of the extracellular space.

In this paper, we describe a special microfluidic device—the NanoPhysiometer (NP)—that allows trapping single cardiac myocytes in a confined sub-nanoliter volume and the measurement of the acidification rate using microfabricated pH sensitive iridium oxide ( $\text{IrO}_x$ ) thin film electrodes on a glass substrate. The glass slide provides the base layer of a microfluidic network made of polydimethylsiloxane (PDMS) with integrated valves to allow control of the fluidic access to the cell detection volume. The device architecture can be easily extended to multiple detection volumes allowing for high throughput measurements.

This device was used to study the physiology of mouse cardiac myocytes with a genetic defect leading to very long chain Acyl-CoA dehydrogenase (VLCAD) deficiency. Patients with VLCAD are at risk for cardiomyopathy, myocardial dysfunction, ventricular tachycardia and sudden cardiac death (BrownHarrison et al., 1996; Scholte et al., 1999; Spiekerkotter, 2006). VLCAD is required to metabolize fatty acid, the preferred substrate of the heart (Wanders et al., 1999). We hypothesize that the VLCAD  $-/-$  phenotype has an increased intracellular acidification rate, which leads to an influx of  $\text{Na}^+$  through the  $\text{Na}^+-\text{H}^+$  exchanger. The resulting increase in  $\text{Na}^+$  leads to an increase in the intracellular  $\text{Ca}^{2+}$  concentration through the  $\text{Na}^+-\text{Ca}^{2+}$  exchanger. Acidosis and  $\text{Ca}^{2+}$  overload also plays a major role in the ischemic myocardium (Kloner and Jennings, 2001b; Kloner and Jennings, 2001a), and our device concept can be easily adapted to study reperfusion injury and identify strategies and possible pharmacological targets for ischemic heart diseases.

## 2 Materials and reagents

Iridium tetrachloride, oxalic acid dehydrate, hydrogen peroxide (30% solution in water) and anhydrous potassium carbonate were purchased from Aldrich. Platinum (99, 95%), rod diam. 2 mm, and titanium (99, 95%), rod diam. 2 mm, were purchased from Goodfellow Corp. For calibration, universal pH buffers were used (buffers for pH 6, 7 and 8 from VWR Scientific, West Chester, PA). The cell culture media were purchased from BioWhittaker. All chemicals were used as received. Double-distilled (DI) water was used for the preparation of all solutions. Polydimethylsiloxane (PDMS) elastomer composed of prepolymer and curing agent was purchased from Essex Chemical (Sylgard 184, Edison, NJ).

## 3 Instrumentation

All electrochemical experiments were performed with a CHI model 660A potentiostat/galvanostat (CH Instruments, Austin, TX) in a three-electrode configuration. In general, the potentials were measured relative to a Ag/AgCl (CHI 111, CH Instruments) reference electrode. The counter electrode was typically a Pt wire with a diameter of 1 mm (CHI 115, CH Instruments). Dri-Ref-450 from World Precision Instrument Inc. was used as reference electrode (diameter 0.45 mm). The  $\text{IrO}_x$  electrode potential was monitored in the open circuit potential (OCP) mode.

We used a stylus surface profiler (Alphastep 200, Tencor Instruments) to measure the thickness of the photoresist layers and iridium oxide films.

An upright optical microscope (OLYMPUS BX-41) with a CCD camera (Micropublisher 3.3, QImagine, Canada) was used to monitor the surface of platinum and iridium oxide electrodes and to align the thin film electrodes relative to the microfluidic flow channels of our PDMS NanoPhysiometer. Fluidic flow visualization was performed using colored solutions and an inverted microscope (AXIOVERT 25CFL, Carl Zeiss, Germany) in combination with a color CCD camera (KP-D20BU, Hitachi, Japan). The same system was used to image the morphology and the contraction of cells in the on-chip cell culture volume. The fluidic flow was controlled and maintained using a microsyringe pump controller MICRO-4 (WPI, Sarasota, FL) with flow rates ranging from 1 to 30 nL/s.

## 4 NanoPhysiometer fabrication

### 4.1 Thin film electrodes fabrication

The microelectrode arrays were fabricated on microscope glass slides ( $76 \times 25 \times 1$  mm, Fisher Scientific), which were cut into small sections of  $25 \times 25$  mm<sup>2</sup>. The glass substrates were cleaned prior to the deposition using a standard cleaning protocol (Henke et al., 2002) as follow: soak 5 min in hexane, 5 min ultrasonic acetone bath, 10 min boiling in isopropyl alcohol. Each cleaning step is completed by a 10 min rinse under running DI water. In order to mediate adhesion, a thin titanium adhesive layer (10–15 nm) was deposited prior to the platinum deposition of the working electrode (100–150 nm). E-beam evaporation (Inotec Corp.) was used to deposit the metals. The deposition parameters were: total gas pressure during deposition— $2 \times 10^{-6}$  Torr, Ti deposition rate—2 nm/s; Pt deposition rate—5 nm/s and substrate temperature—300 K. The deposition rate and the thickness of the films were controlled by a quartz crystal monitor (Maxtek, Inc.). The Ti and Pt films were deposited in a single process. The platinum films were patterned using

a 1- $\mu\text{m}$  thick photoresist (NR7-1000P, Futurrex, Inc.), standard photolithography and ion beam etching. The photoresist was stripped off from the electrodes in acetone or in resist remover PR4 (Futurrex, Inc.) at room temperature. Finally, the surface was thoroughly cleaned with isopropyl alcohol and then rinsed several times with DI water. The electrode array, with sensing areas of  $20 \times 400 \mu\text{m}^2$  and  $20 \times 60 \mu\text{m}^2$ , was then fabricated utilizing electrodeposition of  $\text{IrO}_x$  as described below. A microscope image and a schematic drawing of the electrode geometry are shown in Fig. 1(a) and (b), respectively.

#### 4.2 $\text{IrO}_x$ pH sensitivity and reference electrodes

A detailed protocol to deposit the iridium oxide films onto the Pt-films and their properties was described in previous

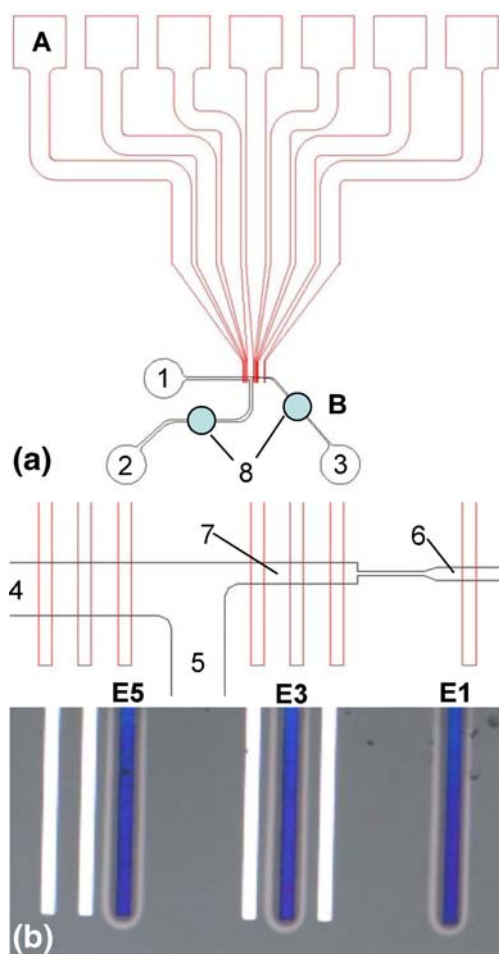


**Fig. 1** (a) Schematic overview of a NanoPhysiometer for acidification rate measurements from single CM cells in sub-nanoliter volumes: (A) microelectrode array; (B) microfluidic channels array; (1) input port; (2) output port; (3) control port; (4) loading channel; (5) output channel; (6) control channel; (7) detection volume; (8) mechanical valve. The inset (a) shows a detailed view of microelectrodes in the detection volume. (b) Optical image of iridium oxide pH sensitive electrodes (E3) and quasi-reference  $\text{IrO}_x$  electrodes (E1 or E5). The width of electrodes is  $20 \mu\text{m}$

work (Ges et al., 2005, 2007). The deposition solution was prepared based on the method proposed by Yamanaka (1989, 1991) and Marzouk et al. (1998; Marzouk, 2003). A Multi-channel CHI 1030 potentiostat was used for the electrochemical deposition of iridium oxide films onto Pt thin film microelectrode arrays in the galvanostatic mode. Dark blue  $\text{IrO}_x$  films (Fig. 1(b)) resulted from a deposition at a constant current density of  $1\text{--}1.5 \text{ mA/cm}^2$ . For a 6–8 min deposition a film thickness of  $100\text{--}120 \text{ nm}$  was obtained. In general, all  $\text{IrO}_x$  thin films on multiple Pt electrodes were formed simultaneously, yielding identical electrochemical characteristics. After electrodeposition the iridium oxide electrodes were rinsed under running distilled water for 5 min and were soaked in a potassium phosphate buffer solution (pH 7.0) for up to 20 h to stabilize the electrodes' characteristics and to reduce potential drifts. To achieve long-term stability,  $\text{IrO}_x$  pH sensitive electrodes were stored in pH 7 buffer solution at room temperature. The sensitivity of these electrodes in the range between pH 4 and 10 demonstrated a linear Nernstian response with a sensitivity of  $70 \pm 5 \text{ mV/pH}$ . The response times of these pH electrodes was in the range of 5–10 s with a baseline drift of 3–5 mV/month.

#### 4.3 PDMS device fabrication

The microfluidic network was fabricated utilizing photolithography and replica molding. Three-inch one-sided polished silicon wafers with a thickness of 0.3 mm (Nova Electronic Materials, Ltd, Carrollton, TX) were cleaned for 10 min in an  $80^\circ\text{C}$   $\text{HCl}/\text{H}_2\text{O}_2/\text{H}_2\text{O}$  solution (a 1:1:5), rinsed in DI water, and dried in nitrogen. The wafer was spin coated with MicroChem SU-8 2015 photoresist (MicroChem Corp, Newton, MA), with a typical thickness of  $20 \mu\text{m}$  (2000 rpm, 30 s), and pre-exposure baked at  $65^\circ\text{C}$  for 1 min and at  $95^\circ\text{C}$  for 2 min on a hot plate. The photoresist was exposed through the chrome mask with a dose of  $160 \text{ mJ/cm}^2$ . After exposure the resist was baked at  $65^\circ\text{C}$  for 1 min and at  $95^\circ\text{C}$  for 2 min on a hot plate. The wafer was developed for 4 min in MicroChem SU-8 developer, rinsed in isopropyl alcohol for 10 s, and blow-dried with nitrogen. To improve the mechanical properties of the SU-8 we performed a hard bake ( $180^\circ\text{C}$ , 20 min).

A PDMS replica was fabricated by pouring the degassed prepolymer/curing agent (10:1 mixture) on the photoresist master and curing it in an oven at  $60^\circ\text{C}$  for 2 h. Access holes to the channels were punched with a sharpened stainless steel pipe (1 mm external diameter). Each microfluidic device was manually aligned relative to the pH electrodes with a stereo microscope, sealed to the glass substrate by self-adhesion, and stabilized with a mechanical clamp. Glass capillaries were inserted into the access holes

to connect the microfluidic channels to syringes in pumps using standard microtubing (0.5 mm inner diameter, Cole Parmer).

#### 4.4 Mechanical valves for flow control

In order to measure acidification rates and characterize the metabolic activity of cells, the flow in microfluidic devices needs to be controlled very precisely. There is a wide range of different valve technologies to control fluid flow and deliver specific amounts of reagents in microfluidic-based cell culture devices. In our application, even small leak rates could lead to large errors, so we decided to implement miniature mechanical screw valves (Weibel et al., 2005). Our design allowed us to place two valves within a footprint of  $6 \times 8 \text{ mm}^2$  in close proximity to the cell trap (Fig. 2(a)). The valves were fabricated by drilling a pocket hole above the microfluidic channel into the PDMS. Into the pocket hole we inserted an oversized threaded sleeve and a screw which allowed us to compress the PDMS beneath the screw and above the microfluidic channel. Figure 2(b), (c) shows the operation of these mechanical

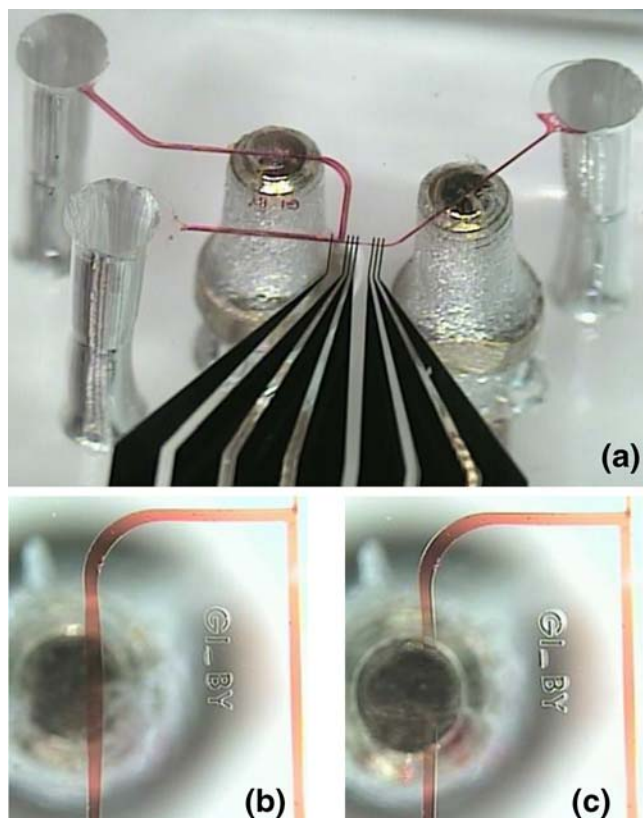


**Fig. 2** Optical images of mechanical valves. (a) Microfluidic device with two valves (black—Pt electrodes; red—microfluidic channels: 100  $\mu\text{m}$  wide, 20  $\mu\text{m}$  tall). (b) Bottom view of a channel containing a dye solution; the valve is open. (c) Bottom view of a channel that has been completely closed by rotating the screw

valves. The functionality and the leak rate of the valves were assessed with a dye solution. Figure 2(b) shows the channel opened and Fig. 2(c) shows the channel closed after rotating the screw. The use of these valves proved essential in obtaining reliable measurements of acidification rates from single cardiac myocyte cells in a confined extracellular space. In microfluidic devices, small pressure gradients will result in unpredictable flow pattern and larger errors.

#### 4.5 NanoPhysiometer assembly

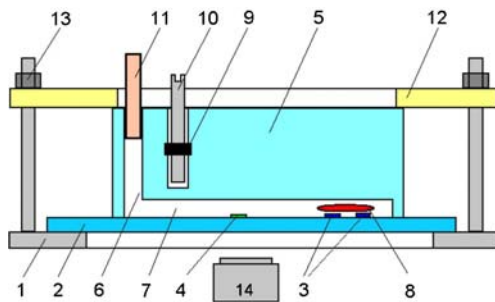
The fabrication of the cardiac NP consists of three major steps: fabrication of the pH sensitive microelectrodes on the glass substrate; molding a PDMS device with the microfluidic channel network, and assembly of the mechanical valves to control the fluid flow. A cross section of the fully assembled device is shown in Fig. 3. For mechanical rigidity and to improve the seal between the PDMS and the glass substrate, a clamp was used to press the PDMS device against the substrate. Glass capillaries with plastic microtubing were inserted into the control and output ports (Figs. 1(a) and 3) and connected to manual syringes for trapping single cells in the detection volume.

Figure 1 shows the layout of the microfluidic device and the sensing electrodes overlaid. The electrode array consists of seven independent electrodes, which were divided into three groups. The distance between the electrodes in each group was 40  $\mu\text{m}$  and the distance between the groups was 200  $\mu\text{m}$ .  $\text{IrO}_x$  films were deposited only onto the tips of the Pt electrodes ( $20 \times 200 \mu\text{m}^2$ ). Depending on the purpose of the experiment, 3 to 7 electrodes were covered by  $\text{IrO}_x$  films. Usually the middle group with three electrodes was positioned in the detection volume (7). The length of the cardiac myocytes (CM) varies from 50 to 150  $\mu\text{m}$ , therefore such an electrode configuration allows us to place the CM on the pH sensitive electrodes within the detection volume.

### 5 Single cell isolation

Mice were anesthetized by intraperitoneal injection of Avertin solution (5 mg Avertin per 10 g body weight, T48402, Sigma-Aldrich) containing heparin (3 mg/10ml, H9399, Sigma-Aldrich). The heart was rapidly excised and placed into ice-cold  $\text{Ca}^{2+}$ -free and glucose-free HEPES-buffered Tyrode's solution (T). The T solution contained (in mM): NaCl—140, KCl—4.5,  $\text{MgCl}_2$ —0.5,  $\text{NaH}_2\text{PO}_4$ —0.4,  $\text{NaHCO}_3$ —10, HEPES—10. The pH of all solutions was adjusted to 7.4 using NaOH.

The aorta was cannulated and the heart was perfused with T solution at room temperature for 10 min to stop contractions. The perfusion was then switched to T solution



**Fig. 3** Cross-sectional schematic of the completely assembled Nano-Physiometer. A clamp ensures mechanical stability of the seal between the PDMS microfluidic device and the electrode arrays. 1—aluminum base; 2—glass substrate; 3—IrO<sub>x</sub> pH sensitive electrode; 4—IrO<sub>x</sub> quasi-reference electrode; 5—PDMS microfluidic device; 6—input port; 7—microchannel (20 μm height); 8—single cardiac myocyte cell; 9—thredded sleeve; 10—microvalve screw; 11—tubing to syringe pump; 12—acrylic cover; 13—screw to adjust pressure; 14—objective

containing 10 μM CaCl<sub>2</sub> with collagenase (178 U/ml, CLS2, Worthington Biochemical) and protease (0.64 U/ml, P5147, Sigma-Aldrich) for 12 min at 37°C. Tissues from the atria and aorta were discarded. Remaining ventricular tissue was coarsely minced and placed into T solution containing 0.5 mM Ca<sup>2+</sup>. Myocytes were dissociated by gentle agitation and used within 3 h after isolation.

## 6 Results and discussion

### 6.1 Characterization of pH microsensors

The IrO<sub>x</sub> films in Fig. 1(b) were deposited simultaneously on multiple platinum electrodes. The iridium oxide films were dark blue or blue in color in the thickness range from 0.1 to 0.12 μm. The initial calibration of our IrO<sub>x</sub> electrodes was made in a beaker, in three different buffer solutions using an external Ag/AgCl reference electrode. Figure 4(a) shows the open circuit potential changes of E1, E3, E5 IrO<sub>x</sub> pH electrodes at different standard pH calibration solutions. All electrodes showed practically identical characteristics with a sensitivity of 72±2 mV/pH. Another important characteristic of the iridium oxide electrodes was their long-term stability, or potential drift. Figure 4(b) shows the long-term stability of the open circuit potential between E1, E3, E5 pH sensitive electrodes and a Ag/AgCl reference electrode in Tyrode's solution, pH 7.3 (cell culture media for CM). The potential drift for these electrodes was less than 1–2 mV over a period of 20 min. We obtained the same characteristics if the calibration of these electrodes was performed in the microfluidic channels (40 μm height and 100 μm width). The sensitivity of the iridium oxide electrodes was not changed for times up to 6 weeks after the deposition. Our freshly deposited electrodes demon-

strated a response time to a change in the pH of the solution by one unit of about 4 s; two weeks after the deposition the average response time was 6–8 s.

In our previous work (Ges et al., 2007), we described a new approach to measure pH differences in microfluidic devices. We used two IrO<sub>x</sub> thin film electrodes: one to sense the pH and the other as quasi-reference. With this configuration, we confirmed experimentally that our pH electrode sensitivity exactly corresponds to the electrode sensitivity obtained using an external Ag/AgCl reference electrode. In this work we also used a differential pH sensing method. In Fig. 1, the IrO<sub>x</sub> pH sensitive electrodes were situated in the detection volume and the IrO<sub>x</sub> quasi-reference electrodes were placed in the loading channel (4) or in the control channel (6) with a distance of at least 200 μm from the pH electrode. The utilization of an IrO<sub>x</sub> thin film electrode as quasi-reference substantially simplifies pH measurement in microfluidic devices. Additional advantages of the IrO<sub>x</sub> sensors are biocompatibility and long-term stability upon exposure to the cell culture media.

After the experiment the NP was disassembled, the PDMS device was swab-cleaned with methyl alcohol and then rinsed in DI water, as were the IrO<sub>x</sub> electrodes, followed by blow-drying with nitrogen for a few minutes. The NP was used multiple times to complete our study.

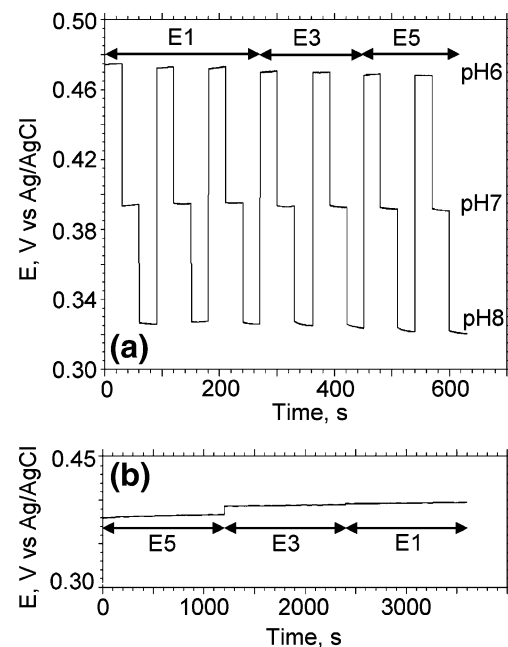


**Fig. 4** (a) Open circuit potential of E1, E3, E5 IrO<sub>x</sub> pH electrodes during periodic cycling of 3 different standard pH calibration solutions versus an external CHI Ag/AgCl reference electrode. The experiments were performed in a beaker with 30 s measurement intervals. (b) Long-term stability measurements (during 20 min) of the open circuit potential between E1, E3, E5 IrO<sub>x</sub> pH electrodes versus a standard reference electrode in a beaker filled with Tyrode's solution at pH 7.4

## 6.2 NanoPhysiometer single cell manipulation

Since our glass substrates and PDMS elastomer (thickness 5–6 mm) are transparent, the detection volume and microfluidic channel can be imaged from both the top and the bottom of the device. The 5  $\mu\text{l}$  input port was used as a cell reservoir. A concentrated cell suspension (2–3  $\mu\text{l}$ ) was added to the input port (Fig. 1(a)) using a syringe with a plastic needle. The input port (1) is connected to the 0.36 nL single cell detection volume (7) through the cell loading channel. By applying a pressure gradient to the output port, the CM cells move from the reservoir toward the detection volume along the loading channel. If the cell was in close proximity to the detection volume, a negative pressure was applied to the control port to position the cell above the sensors. In order to suppress residual flow, we then closed the mechanical valves blocking the output and control channels to start the acidification rate measurements. The trapping of the cells in the detection volume takes 2–5 min after loading cell suspension into the input port. Generally our cell viability was larger than 20%. Under our conditions CM are viable in the NP for 5–6 h, but we aimed to complete our experiments within 1–2 h after isolation.

To obtain reproducible results, we developed a special protocol for acidification rate measurements: (1) align the glass substrate with the pH sensitive electrode array and the PDMS microfluidic device; (2) install the microfluidic device in the clamping mechanism to provide mechanical rigidity and to prevent cell media leaks; (3) calibrate the iridium oxide electrodes using two standard buffer solutions with different pH (usually pH 7 and 8); (4) evaluate the potential drift in cell media for 30 min; (5) clean the microfluidic channels with DI water; (6) pipette the CM cells into the input port of the microfluidic device and apply pressure gradients between the output and control ports to trap the single cells above the pH electrode; (7) close the control and output channels using the screw valves to suppress residual fluid flow in the sensing volume; (8) measure the acidification rate of CM cell after equilibrium conditions are reached; (9) open the control and output channels to remove cells from the detection volume by applying negative pressure to the output channel; (10) load new CM cells into the sensing volume and repeat steps 7–11.

## 6.3 Acidification rate measurements from single cardiac cells

The metabolic activity and the physiological state of living cells can be characterized by the rate at which cells generate acidic byproducts. In order to investigate if a differential sensing scheme could be used, we performed acidification measurements on single cardiac myocytes utilizing a macro-

scopic Dri-Ref-450 Ag/AgCl reference electrode and a quasi-reference  $\text{IrO}_x$  electrode. Figure 5 shows the OCP between an  $\text{IrO}_x$  electrode (3) located in the detection volume referenced to a quasi-reference  $\text{IrO}_x$  electrode in the cell loading channel (5) and subsequently referenced to an external Ag/AgCl reference electrode (R) inserted in the input port during the time course of one experiment. During this experiment, we also recorded the OCP between the quasi-reference electrode and the Ag/AgCl reference electrode.

After closing the valves, a large drift in the open circuit potential of 20–100 s duration is typically observed in the OCP independent of the type of reference electrode used. This drift is most likely associated with the residual flow in the microfluidic device. After about 100 s the change in pH remains constant over time and the slope of the OCP represents the acidification rate. For the quasi-reference electrode configuration we computed an acidification rate of 13 mpH/min (trace 3–5). After 5 min we switched the reference electrode to the macroscopic Ag/AgCl electrode in the cell input port and recorded the OCP. After a much shorter initial stabilization period the acidification rate stayed constant and was computed as 15 mpH/min (trace 3-R). To confirm that the quasi-reference electrode remains at constant pH, we recorded the OCP between the quasi-reference electrode and the Ag/Cl reference electrode (trace 5-R). The corresponding change in pH corresponds to  $\sim 0.2$  mpH/min and is comparable to the drift we observed in beaker experiments using standard buffer solutions.

Both measurements are in good agreement and indicate that in our experimental geometry the single cell can not be modeled as a point source for protons, which would result in a negligible differential due to the large diffusion coefficient and the short distance between the sensing electrode and the quasi-reference electrode. Due to a

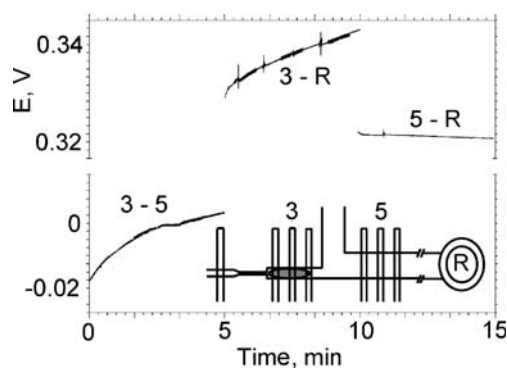


**Fig. 5** Open Circuit Potentials during acidification rate measurements from a single cardiac myocyte with different electrode sensing configurations. The electrodes are labeled: (3)  $\text{IrO}_x$  electrode in the detection volume, (5) quasi-reference  $\text{IrO}_x$  electrode in the cell loading channel and (R) Ag/AgCl Dri-Ref-450 electrode in the cell input port (see insert). The time traces are labeled according to the electrode pair used to record the OCP. The distance between electrodes 3 and 5 is 200 micrometer and 3 mm between 3 and R

comparable diameter of our cell trap and the cardiac myocytes the cross sectional area for the diffusional exchange is small (see image inserted into Fig. 6). Furthermore, the Na<sup>+</sup>/H<sup>+</sup> exchanger is localized at the intercalated disks (faces of the brick shaped cardiac myocytes) and the transverse tubules (Petrecca et al., 1999). The tubules are hollow vessels perpendicular to the longitudinal surface and occupy a 64% of the total surface membrane (Soeller and Cannell, 1999) leaving only approximately 2% for the intercalated disk facing quasi-reference electrode. Therefore, the proton flux over the cell surface is inhomogeneous and hypothesized to be dominated by circumference in close proximity of our IrO<sub>x</sub> sensing electrodes raising the pH locally as confirmed by our measurements. However, due to the slightly variable size of the cardiomyocytes the measured acidification rates might be convoluted by the crosssectional area and we expect these variations to be constant if larger numbers of cardiac myocytes are investigated from different phenotypes.

Therefore, to demonstrate the ability of the Nanophysio-meter to differentiate the acidification rate as a function of extracellular calcium concentrations and between a phenotype with a metabolic deficiency and control, which is hypothesized to change the acidification rate, we conducted experiments on VLCAD deficient (-/-) murine cardiac myocytes and compared these to control (WT).

Figures 6 and 7 show a typical time course of the open circuit potential of the IrO<sub>x</sub> pH microelectrode during the acidification rate measurement from a single wild-type (Fig. 6) and VLCAD -/- (Fig. 7) myocyte trapped above the pH electrode in the detection volume.

Throughout the measurements spontaneous contractions for both types of CM cells were observed. The arrows (Fig. 6) show when these contractions take place in the time course

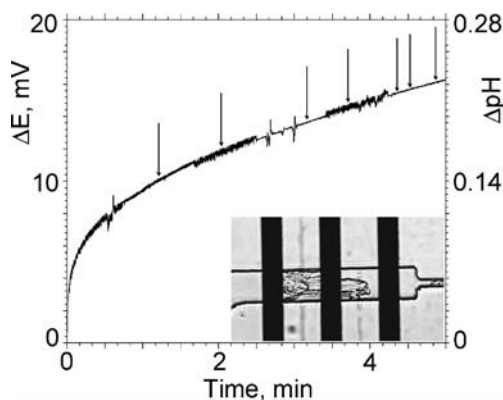


**Fig. 6** Open circuit potential between IrO<sub>x</sub> pH (E3) sensitive and the IrO<sub>x</sub> quasi-reference (E5) electrode for acidification rate measurements of the wild-type cardiac myocyte single cell in 0.36 nL volume in normal Tyrode's solution with 1.8 mM Ca<sup>2+</sup>. The arrows specify the moment of time when spontaneous contraction takes place. The inset shows a detailed view of the cardiac myocyte cell in the cell trap volume in the initial stage of experiment

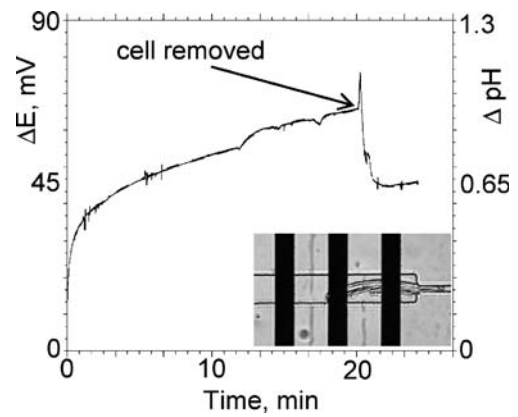


**Fig. 7** Open circuit potential between IrO<sub>x</sub> pH (E3) sensing and the IrO<sub>x</sub> quasi-reference (E1) electrode for acidification rate measurements from a VLCAD cardiac myocyte single cell in Tyrode's solution (1.8 mM Ca<sup>2+</sup> concentration)

of the measurement. The frequency of contraction varied for different cells and exhibited contractions of 0.2–1 Hz or single contractions with periodicity of 1–2 contractions per minute. We didn't find any correlation in the pH signal of CM cells and the spontaneous contractions, which is consistent with the intracellular buffer capability and the second's time constant of our IrO<sub>x</sub> electrodes.

The curves in Figures 6 and 7 can be separated in two regions, where the time course of the OCP is different. After closing the valves, a large drift in the open circuit potential of up to 2 min duration is observed. This drift is most likely associated with the residual flow in the microfluidic device. The second region (2–20 min) is characterized by a constant slope.

To avoid flow artifacts and large deviations from homeostasis, we computed the acidification rates in the linear region from 2 to 20 min for VLCAD -/- and WT

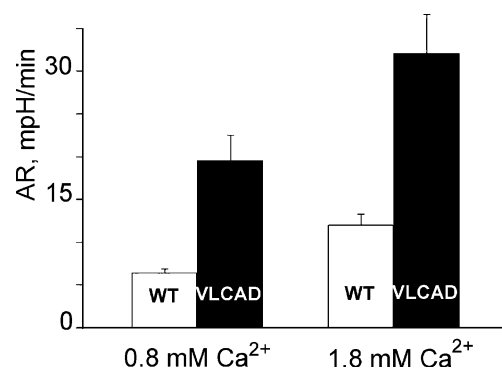


**Fig. 8** Calcium-dependent acidification rate in two types of cardiomyocytes. Cardiomyocytes from VLCAD mice have an average acidification rate of 19.5 ± 3.0 mpH/min (n=4) in 0.8 mM Ca<sup>2+</sup>, which is significantly different from WT cardiomyocytes (t test p<0.00003), with an acidification rate of 6.45 ± 0.38 mpH/min (n=8). In higher Ca<sup>2+</sup> concentration (1.8 mM), differences between the two types of cardiomyocytes are also significant (t test p<0.00004), and acidification rate was 11.96 ± 1.33 mpH/min (n=9) and 32.0 ± 4.64 mpH/min (n=3) for WT and VLCAD cardiomyocytes, respectively

cells. The acidification rate is calculated from the change in OCP over time divided by the sensitivity of the pH electrode. We conducted and analyzed more than forty experiments with single CM cells. In those experiments we monitored pH changes as a result of metabolic activity of the two genotypes of CM cells at normal (1.8 mM) and at a ~twofold decreased (0.8 mM)  $\text{Ca}^{2+}$  concentration in the Tyrode's solution. The analyzed data for the two phenotypes are shown in Fig. 8. The average acidification rate (AR) for the wild-type cardiomyocytes was  $6.45 \pm 0.38$  mpH/min ( $n=8$ ) for 0.8 mM  $\text{Ca}^{2+}$  and  $11.96 \pm 1.33$  mpH/min ( $n=9$ ) for 1.8 mM  $\text{Ca}^{2+}$ . The observed higher metabolic activity at higher  $\text{Ca}^{2+}$  levels is consistent with measurements in whole heart preparations (Marquez et al., 1997). Ganitkevich et al. (2006) published acidification rates measured on single cardiac myocytes in comparable volumes under hypoxic conditions in 1.2 mMol  $\text{Ca}^{2+}$  (Fig. 2D). Based on these data, we computed an acidification rate of approximately 100 mpH/min, which is consistent with our data and the assumption of an approximately sixfold to sevenfold decreased acidification rate in case of aerobic respiration. VLCAD CM cells produce significantly higher values, 19.50 and 32.02 mpH/min, respectively. Thus, at the same  $\text{Ca}^{2+}$  concentration the AR of VLCAD  $-/-$  cells is 2.5–threefold higher than that of the WT. The significantly increased acidification rate supports our hypothesis that in VLCAD  $-/-$  cells the intracellular acidification rate is increased and/or the  $\text{Na}^+/\text{H}^+$  exchanger is more active. The extrusion of protons leads to an influx of  $\text{Na}^+$ , which activates the  $\text{Na}^+/\text{Ca}^{2+}$  exchanger and leads to the observed higher intracellular  $\text{Ca}^{2+}$  levels (Werdich et al., 2007).

## 7 Conclusion

We have developed a microfluidic device platform for the measurement of acidification rates of single cardiac myocytes confined in sub-nanoliter volumes. The device utilizes a differential potentiometric sensing configuration with two thin film  $\text{IrO}_x$  pH electrodes on a glass substrate. A microfluidic network with integrated valves is sealed to the substrate and allows trapping of cardiac myocytes in the detection volume. The VLCAD deficient cells showed a 1.6- to 2.5-fold increase in acidification rate, consistent with our hypothesis of a  $\text{Na}^+/\text{H}^+$  exchanger-induced  $\text{Ca}^{2+}$  load, as observed previously. This approach can easily be extended to study ischemia/reperfusion injury or to disorders of other biological systems.

**Acknowledgments** We thank V. J. Exil for helpful discussions and the generous supply of the VLCAD  $-/-$  mice. This work was

supported in part by the Vanderbilt Institute for Integrative Biosystems Research and Education (VIIBRE) and NIH grant 5U01AI061223-03.

## References

- C.D.T. Bratten, P.H. Cobbold, J.M. Cooper, *Anal. Chem.* **70**(6), 1164–1170 (1998)
- M.C. BrownHarrison, M.A. Nada, H. Sprecher, C. VianeySaban, J. Farquhar, A.C. Gilladoga, C.R. Roe, *Biochem. Mol. Med.* **58**(1), 59–65 (1996)
- X.X. Cai, N. Klauke, A. Glidle, P. Cobbold, G.L. Smith, J.M. Cooper, *Anal. Chem.* **74**(4), 908–914 (2002)
- W. Cheng, N. Klauke, H. Sedgwick, G.L. Smith, J.M. Cooper, *Lab Chip.* **6**(11), 1424–1431 (2006)
- S.E. Eklund, D.E. Cliffl, E. Kozlov, A. Prokop, J. Wiksw, F. Baudenbacher, *Anal. Chim. Acta.* **496**(1–2), 93–101 (2003)
- V. Ganitkevich, S. Reil, B. Schwethelm, T. Schroeter, K. Benndorf, *Circ. Res.* **99**(2), 165–171 (2006)
- I.A. Ges, B.L. Ivanov, D.K. Schaffer, E.A. Lima, A.A. Werdich, F.J. Baudenbacher, *Biosens. Bioelectron.* **21**(2), 248–256 (2005)
- I.A. Ges, B.L. Ivanov, A.A. Werdich, F.J. Baudenbacher, *Biosens. Bioelectron.* **22**(7), 1303–1310 (2007)
- F. Hafner, *Biosens. Bioelectron.* **15**(3–4), 149–158 (2000)
- L. Henke, N. Nagy, U.J. Krull, *Biosens. Bioelectron.* **17**(6–7), 547–555 (2002)
- R.A. Kloner, R.B. Jennings, *Circulation* **104**(24), 2981–2989 (2001a)
- R.A. Kloner, R.B. Jennings, *Circulation* **104**(25), 3158–3167 (2001b)
- L. Lorenzelli, B. Margesin, S. Martinoia, M.T. Tedesco, M. Valle, *Biosens. Bioelectron.* **18**(5–6), 621–626 (2003)
- M.T. Marquez, A. Consolini, P. Bonazzola, J.E. PonceHornos, *Acta Physiol. Scand.* **160**(3), 229–233 (1997)
- S.A.M. Marzouk, *Anal. Chem.* **75**(6), 1258–1266 (2003)
- S.A.M. Marzouk, S. Ufer, R.P. Buck, T.A. Johnson, L.A. Dunlap, W. E. Cascio, *Anal. Chem.* **70**(23), 5054–5061 (1998)
- J.C. Owicki, L.J. Bousse, D.G. Hafeman, G.L. Kirk, J.D. Olson, H.G. Wada, J.W. Parce, *Annu. Rev. Biophys. Biomol. Struct.* **23**, 87–113 (1994)
- W.J. Parak, S. Dannohl, M. George, M.K. Schuler, J. Schaumburger, H.E. Gaub, O. Muller, W.K. Aicher, *J. Rheumatol.* **27**(10), 2312–2322 (2000)
- K. Petrecca, R. Atanasiu, S. Grinstein, J. Orłowski, A. Shrier, *Am. J. Physiol.* **276**(2), H709–H717 (1999)
- H.R. Scholte, R.N.A. Van Coster, P.C. de Jonge, B.J.H.M. Poorthuis, J.A.L. Jeneson, B.S. Andresen, N. Gregersen, J.B.C. de Klerk, H.F.M. Busch, *Neuromuscul. Disord.* **9**(5), 313–319 (1999)
- J. Shim, T.F. Bersano-Begey, X.Y. Zhu, A.H. Tkaczyk, J.J. Linderman, S. Takayama, *Current Topics in Medicinal Chemistry.* **3**(6), 687–703 (2003)
- C. Soeller, M.B. Cannell, *Circ. Res.* **84**(3), 266–275 (1999)
- U. Spiekerkötter, *Mon. Schr. Kinderheilkd.* **154**(12), 1231–1242 (2006)
- E. Thedinga, A. Kob, H. Holst, A. Keuer, S. Drechsler, R. Niendorf, W. Baumann, I. Freund, M. Lehmann, R. Ehret, *Toxicol. Appl. Pharmacol.* **220**(1), 33–44 (2007)
- R.J.A. Wanders, P. Vreken, M.E.J. den Boer, F.A. Wijburg, A.H. van Gennip, L. Ijlst, *J. Inherit. Metab. Dis.* **22**(4), 442–487 (1999)
- D.B. Weibel, M. Kruithof, S. Potenta, S.K. Sia, A. Lee, G.M. Whitesides, *Anal. Chem.* **77**(15), 4726–4733 (2005)
- A.A. Werdich, F. Baudenbacher, I.A. Dzura, A. Anderson, V. Ecel, *Am. J. Physiol. Heart Circ. Physiol.* **292**, H2202–H2211 (2007)
- K. Yamanaka, *Jpn. J. Appl. Phys. & Review Papers* **28**(4), 632–637 (1989)
- K. Yamanaka, *Jpn. J. Appl. Phys. & Review Papers* **30**(6), 1285–1289 (1991)